Dielectric-lined cylindrical metallic THz waveguides: mode structure and dispersion

Oleg Mitrofanov[1]* and James A. Harrington[2]

[1]*Department of Electronic and Electrical Engineering, University College London, Torrington Place, WC1E 7JE, UK*
[2]*Department of Material Science & Engineering, Rutgers University, 607 Taylor Rd. Piscataway, NJ 08854, USA*
**o.mitrofanov@ucl.ac.uk*

Abstract: Thin dielectric layers deposited on the inner surface of hollow cylindrical metallic waveguides for Terahertz (THz) waves reduce transmission losses below 1 dB/m. Impact of the dielectric layer on the waveguide dispersion is experimentally investigated by near-field mapping of guided short THz pulses at the input and the output of the waveguide. We obtain dispersion characteristics for the low-loss waveguide modes, the linearly-polarized HE_{11} mode and the TE_{01} mode, and compare the experimental results to the metallic waveguide dispersion. The additional dispersion due to the dielectric layer is found to be small for the HE_{11} mode and the phase velocity is primarily determined by the waveguide radius.

OCIS codes: (230.7370) Waveguides; (300.6495) Spectroscopy, terahertz; (110.6795) Terahertz imaging; (320.0320) Ultrafast optics.

References and links

1. B. Bowden, J. A. Harrington, and O. Mitrofanov, "Silver/polystyrene-coated hollow glass waveguides for the transmission of terahertz radiation," Opt. Lett. **32**(20), 2945–2947 (2007).
2. Y. Matsuura, and E. Takeda, "Hollow optical fibers loaded with an inner dielectric film for terahertz broadband spectroscopy," J. Opt. Soc. Am. B **25**(12), 1949–1954 (2008).
3. K. Nielsen, H. K. Rasmussen, A. J. Adam, P. C. Planken, O. Bang, and P. U. Jepsen, "Bendable, low-loss Topas fibers for the terahertz frequency range," Opt. Express **17**(10), 8592–8601 (2009).
4. C.-H. Lai, Y.-C. Hsueh, H.-W. Chen, Y. J. Huang, H. C. Chang, and C.-K. Sun, "Low-index terahertz pipe waveguides," Opt. Lett. **34**(21), 3457–3459 (2009).
5. M. Miyagi, and S. Kawakami, "Design theory of dielectric-coated circular metallic waveguides for infrared transmission," J. Lightwave Technol. **2**(2), 116–126 (1984).
6. X.-L. Tang, Y.-W. Shi, Y. Matsuura, K. Iwai, and M. Miyagi, "Transmission characteristics of terahertz hollow fiber with an absorptive dielectric inner-coating film," Opt. Lett. **34**(14), 2231–2233 (2009).
7. J. W. Carlin, and P. D'Agostino, "Normal Modes in Overmoded Dielectric-Lined Circular Waveguide," Bell Syst. Tech. J. **52**, 453–486 (1973).
8. C. Dragone, "Attenuation and Radiation Characteristics of the HE_{11} Mode," IEEE Trans. Microw. Theory Tech. **28**(7), 704–710 (1980).
9. C. Themistos, B. M. A. Rahman, M. Rajarajan, K. T. V. Grattan, B. Bowden, and J. A. Harrington, "Characterization of silver/polystyrene-coated hollow glass waveguides at THz frequency," J. Lightwave Technol. **25**(9), 2456–2462 (2007).
10. O. Mitrofanov, T. Tan, P. R. Mark, B. Bowden, and J. A. Harrington, "Waveguide mode imaging and dispersion analysis with terahertz near-field microscopy," Appl. Phys. Lett. **94**(17), 171104 (2009).
11. N. C. J. van der Valk, and P. C. M. Planken, "Effect of a dielectric coating on terahertz surface plasmon polaritons on metal wires," Appl. Phys. Lett. **87**(7), 071106 (2005).
12. M. Gong, T.-I. Jeon, and D. Grischkowsky, "THz surface wave collapse on coated metal surfaces," Opt. Express **17**(19), 17088–17101 (2009).
13. B. Bowden, J. A. Harrington, and O. Mitrofanov, "Low-loss modes in hollow metallic terahertz waveguides with dielectric coatings," Appl. Phys. Lett. **93**(18), 181104 (2008).
14. B. Bowden, J. A. Harrington, and O. Mitrofanov, "Fabrication of terahertz hollow-glass metallic waveguides with inner dielectric coatings," J. Appl. Phys. **104**(9), 093110 (2008).
15. O. Mitrofanov, M. Lee, J. W. P. Hsu, I. Brener, R. Harel, J. Federici, J. D. Wynn, L. N. Pfeiffer, and K. W. West, "Collection mode near-field imaging with 0.5 THz pulses," IEEE J. Sel. Top. Quantum Electron. **7**(4), 600–607 (2001).
16. O. Mitrofanov, I. Brener, M. Wanke, R. R. Ruel, J. D. Wynn, A. J. Bruce, and J. Federici, "Near-field microscope probe for far infrared time domain measurements," Appl. Phys. Lett. **77**(4), 591–593 (2000).

#119824 - $15.00 USD Received 10 Nov 2009; revised 4 Dec 2009; accepted 5 Dec 2009; published 15 Jan 2010

1. Introduction

Development of low-loss and low-dispersion waveguides for Terahertz (THz) waves is challenging. Practical THz waveguides with losses below the level of 1 dB/m only recently have been realized [1–4]. In cylindrical hollow metallic waveguides, the minimal loss can be achieved if a thin (~λ/10) dielectric coating is added to the inner waveguide wall [5–9]. The reduced absorption is a result of a change in the waveguide dominant mode structure. Distinctly different from the dominant mode in the metallic waveguide (TE_{11}), the dominant mode in the dielectric-lined guide (HE_{11}) exhibits minimal penetration into the absorbing metallic wall. The transformation of the dominant mode was recently confirmed experimentally by mapping the mode profile at the waveguide output [10].

The presence of the dielectric layer however raises questions about its effect on group velocity dispersion. In fact, the addition of a dielectric layer can significantly deteriorate group velocity characteristics for some modes, as it does in dielectric-coated surface plasmon waveguides [11,12]. The effect of the dielectric however could be small for the dominant HE_{11} mode because only a small fraction of the wave propagates in the dielectric when the loss is minimal. There are analytical methods for dispersion estimation in the dielectric-lined waveguides. However they rely on mathematical approximations, which need to be verified.

Here we determine the waveguide dispersion characteristics and evaluate the effect of the dielectric layer experimentally. We consider polystyrene-coated hollow cylindrical silver (Ag/PS) waveguides [1]. For a multimode waveguide, characterization of dispersion requires knowledge of mode composition at the input and the output of the test waveguide. We recently showed that the required information can be obtained using THz near-field microscopy [10]. This method is applied here to identify the propagating modes at the input and the output of the tested waveguides. We first allow the waveguide modes to form in the launch waveguide. Spectroscopic analysis is then performed using THz time-domain spectroscopy together with monitoring the mode structure at the input and the output of the test waveguide positioned immediately after the launch guide. This approach allows us to obtain mode-specific dispersion characteristics in a wide range of frequencies.

Two modes in the dielectric-coated cylindrical metallic waveguide are considered: the hybrid linearly-polarized HE_{11} mode and the azimuthally polarized TE_{01} mode. These modes experience small absorption due to vanishing electric field at the waveguide wall [13]. The HE_{11} mode has the lowest transmission loss and very high coupling efficiency to free-space propagating beams [13]. The TE_{01} mode, the lowest-loss mode in metallic waveguides, is considered for comparison.

We provide dispersion characteristics for the HE_{11} and TE_{01} modes and show that the effect of the dielectric layer on phase velocity is small for these modes. However, the linearly-polarized HE_{11} mode has an unusual cut-off frequency behavior, substantially different from the dominant TE_{11} mode in metallic waveguides. The TE_{01} mode on the other hand follows characteristics of the TE_{01} mode in a metallic waveguide very closely within the full range of measured frequencies (0.5-3.0 THz). We also show that the propagation constants can be approximated by analytical functions in the low-loss region suggesting that the effect of the dielectric coating for these modes can be treated by the perturbation theory.

2. Analysis of the mode structure

The waveguides are fabricated by coating the inner surface of 1.8 ± 0.05 mm bore diameter glass tubes with layers of silver (Ag) and polystyrene (PS). The thickness of the Ag and PS coatings are 1 μm and 14 ± 4 μm respectively. Fabrication details are described in Ref. 14. The waveguides exhibit a transmission loss minimum for the HE_{11} mode in the region of 2-3 THz [1,13]. Short THz pulses are generated in a ZnTe crystal by optical rectification of 100-fs pulses from a Ti:Sapphire laser. After passing through a 3-mm thick Si plate, which blocks the laser beam, a portion of the unfocused THz beam couples into the waveguide through a 1-mm diameter pinhole in a thin stainless steel screen positioned in contact with the waveguide input. After propagation through the waveguide (filled with air at ~50% RH), the THz wave is

#119824 - $15.00 USD Received 10 Nov 2009; revised 4 Dec 2009; accepted 5 Dec 2009; published 15 Jan 2010

detected in the near-field zone (within ~100 μm) of the waveguide output by an integrated near-field probe with a 50 μm aperture [15]. The probe detects the horizontal component of the electric field. To visualize the propagating modes, space-time maps of the electric field are measured along the waveguide diameter.

Desired modes can be excited by controlling the input field pattern formed by the pinhole. The THz pulse energy is distributed between the modes in a way that their superposition is matched to the incident field pattern. The HE_{11} mode is launched through the input pinhole centered on the waveguide axis [schematic diagram, Fig. 1(a)]. Coupling to higher order modes in this case is small. Figure 1(a) shows the space-time map of the output THz wave after propagation in a 133.5-mm long Ag/PS waveguide. The field pattern in the region around $t = 0$ corresponds to the HE_{11} mode. The map also shows that several waveguide modes are excited and the higher order modes arrive a few picoseconds later, however most of the wave energy is in the dominant HE_{11} mode.

A different arrangement is required for excitation of the TE_{01} mode, for which the electric field lines describe concentric circles around the waveguide axis. The mode symmetry prohibits coupling of a linearly-polarized beam into this mode if the pinhole is centered on the waveguide axis. In order to excite the TE_{01} mode the input pinhole is shifted to the waveguide wall and the polarization of the incident field is rotated by 90 degrees [schematic diagram, Fig. 1(b)]. This arrangement launches the TE_{01} mode without significant coupling to the HE_{11} mode. After propagation in the waveguide, the mode fully develops its horizontally-polarized component at the output. To detect the TE_{01} mode the horizontally polarized electric field is measured along the vertical line passing through the waveguide axis. Figure 1(b) shows the output wave map with an anti-symmetric pattern corresponding to the TE_{01} mode.

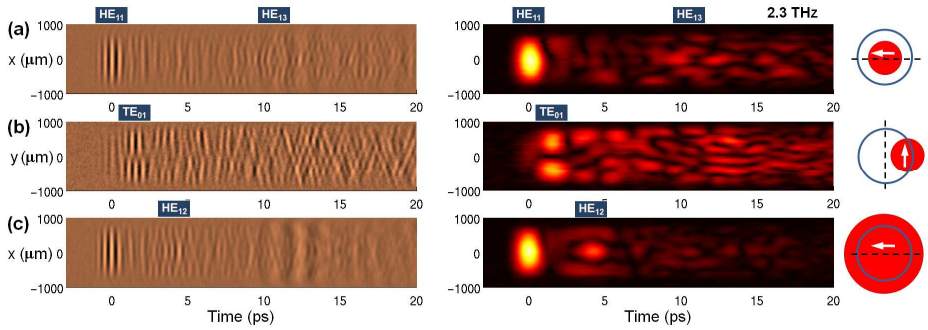

Fig. 1. Space-time maps of the THz wave coupled to different combinations of waveguide modes. Maps of the electric field $E_x(t)$ are shown in the left column and the corresponding maps of the field amplitude $E_x(\omega)$ at 2.3 THz are shown in the right column. The position of the input pinhole, the incident field polarization and the spatial scan lines are schematically shown on the right.

The mode symmetry and location on the time-space map become more obvious after performing local Fourier transforms with the 2-ps long Hann window [10]. It allows plotting distribution of the spectral amplitude at a selected frequency. The right column maps in Fig. 1 show the distribution at the spectral maximum (2.3 THz) calculated directly from the data. The HE_{11} and the TE_{01} modes clearly appear as temporally confined packets of energy. The higher order modes are characterized by several nodes in the transverse direction and lower group velocities. The HE_{12} mode for example is delayed by ~4 ps. This mode clearly shows if the incident field illuminates the core of the waveguide uniformly [Fig. 1(c)] [10]. Note that the $t = 0$ point in all maps marks the arrival time for the HE_{11} mode, which is delayed by 1.3 ps with respect to the arrival time of the wave in free space.

The excited modes become separated in time when they arrive at the waveguide output. Therefore mode profiles can be determined by mapping the electric field distribution at the moment of arrival. Two-dimensional distributions of the electric field component E_x are shown in Fig. 2(a) for the following time-delays: $t = 0$, 1.5, 4.2, and 10.2 ps. In addition to the

#119824 - $15.00 USD Received 10 Nov 2009; revised 4 Dec 2009; accepted 5 Dec 2009; published 15 Jan 2010

HE_{11} mode profile, first shown in Ref. 10, field patterns of higher order modes can be clearly identified as the TE_{01}, HE_{12} and HE_{13} modes after comparing the profiles to analytical approximations shown in Fig. 2(b). The HE_{1m} modes are linearly polarized and the orthogonal component E_y is zero. The azimuthally polarized TE_{01} mode has the orthogonal E_y component that shows a similar spatial distribution as E_x but rotated around the waveguide axis by 90 degrees (not shown).

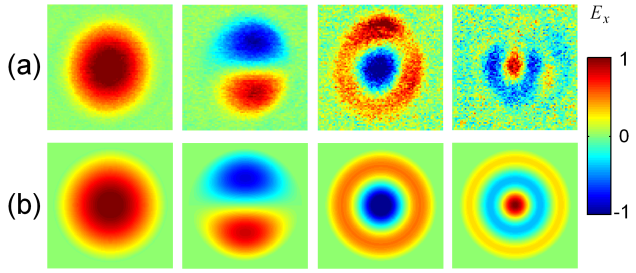

Fig. 2. Spatial distribution of normalized electric field E_x for the modes in the dielectric-lined cylindrical metallic waveguide: HE_{11}, TE_{01}, HE_{12}, and HE_{13} (from left to right). Experimental profiles (a) are measured at t = 0, 1.5, 4.2, and 10.2 ps respectively. Each map shows a 2x2 mm^2 area for the 1.8-mm diameter waveguide. Analytical approximations are shown in (b).

3. Dispersion characteristics of the HE_{11} and TE_{01} modes

After establishing the mode structure and composition we can address dispersion characteristics. Figure 1(a) and 1(b) showed that a large portion of the wave energy can be coupled in either the HE_{11} or the TE_{01} mode. The quasi single-mode propagation helps determine dispersion relations for these modes. In the experiment two waveguide sections are positioned in series: one serving as the launch waveguide and the other as the test waveguide. The THz pulse is then mapped at the output of the test waveguide and compared to the pulse at the output of the launch waveguide. The dispersion relationship for the test waveguide now can be determined by performing the Fourier transforms of the input and output waveforms and obtaining their phase difference for each frequency component. The corresponding phase velocity plots are summarized in Fig. 3.

First we compare the dispersion characteristics in an uncoated silver guide with the theory for the classical TE_{11} mode to verify the characterization method. The TE_{11} mode is formed at the end of a 142-mm-long launch Ag guide illuminated uniformly by the unfocused THz beam. After propagation through a 151-mm-long test Ag waveguide the THz pulse is measured in the center of the output. The pulse waveform is also measured in the far-field zone by a photoconductive antenna [16] equipped with a 1-mm radius hyper-hemispherical silicon lens (at a distance of 10 mm from the guide output). The input waveforms for the test guide are obtained at the output of the launch waveguide. Phase velocity plots extracted from both the near-field and the far-field measurements show excellent agreement with the exact theory for a perfect-metal waveguide (Fig. 3) confirming that the characterization method is reliable. Note that the phase error caused by the presence of higher order modes is not significant.

#119824 - $15.00 USD Received 10 Nov 2009; revised 4 Dec 2009; accepted 5 Dec 2009; published 15 Jan 2010

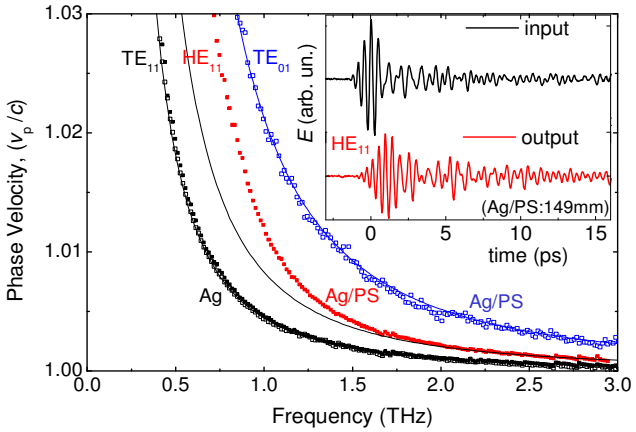

Fig. 3. Phase velocity plots for the HE_{11} and TE_{01} modes in the dielectric-coated (Ag/PS) waveguide and for the TE_{11} mode in the metallic (Ag) waveguide. Solid and empty symbols show the experimental data measured in the far-field (ff) and near-field (nf) zones respectively. Solid lines show the exact analytical solutions for the TE_{11} and TE_{01} modes in the metallic waveguide and the approximation for the HE_{11} mode. The inset shows waveforms of the input and output THz pulses propagating as the HE_{11} mode in the Ag/PS guide.

Next we consider the TE_{01} mode in the dielectric-coated waveguide. For this mode the far-field measurement is not simple because of the mode symmetry. The input and the output waveforms however can be detected in the near-field zone at the mode maximum, located close to the half-radius point along the vertical axis (y = 0.45 mm). A 133.5-mm-long waveguide section is used as the launch waveguide and a 149-mm-long section as the test waveguide.

To evaluate the effect of the dielectric layer we compare the phase velocity data with the theoretical dispersion curve for the TE_{01} mode in the uncoated metallic waveguide (Fig. 3). The phase velocity is determined by the bore radius a in the metallic waveguide. It can be expressed in terms of the TE_{01} cutoff frequency $f_c = \omega_c/2\pi = 3.832 \cdot c/(2\pi a) = 0.203$ THz:

$$v_p = c \cdot \left(1 - \frac{\omega_c^2}{\omega^2}\right)^{-1/2} . \qquad (1)$$

The experimental data for the dielectric-lined guide follows this phase velocity relation. The dielectric layer therefore produces no noticeable effect on dispersion for this mode. The result is consistent with the fact that only a small fraction of the wave travels in the dielectric.

Finally we consider the dominant HE_{11} mode. Unlike the TE_{01} mode, the HE_{11} mode couples very efficiently into free space [13]. The input and output waveforms for this mode are therefore obtained using the far-field detector with a silicon lens (Fig. 3, inset). This arrangement gives a higher signal-to-noise ratio. The phase velocity plot for this mode (Fig. 3) exhibits a diverging behavior at low frequencies similar to the other modes. However the experimental data noticeably deviates from the standard cutoff frequency behavior of Eq. (1).

To explain this behavior we consider the relationship between the spatial mode profile and the cutoff frequency. The mode profile is determined by the transverse component of the mode wavevector k_t, which is proportional to the cutoff frequency $\omega_c = k_t c$. The mode profiles in Fig. 2(a) therefore can be used to determine the corresponding cutoff frequencies. We first compare the detected profiles with an approximate solution derived by Miyagi and Kawakami for the hybrid modes in the case of the transmission loss minimum [5]. The detected profiles agree with the approximation shown in Fig. 2(b). Therefore the characteristic k_t can be found directly from the approximation. In particular, the Cartesian components for the HE_{11} mode:

$$E_x(r,\theta) = E_0 J_0(k_t r); \qquad E_y(r,\theta) = 0; \qquad (2)$$

#119824 - $15.00 USD Received 10 Nov 2009; revised 4 Dec 2009; accepted 5 Dec 2009; published 15 Jan 2010

where J_0 is the Bessel function of the zeroth order, and E_0 is the electric field amplitude at the waveguide center [5]. The minimum-loss condition requires that the electric field is zero at the metallic wall: $E_x = E_y = 0$ at $r = a$. The corresponding value of k_t therefore must be given by the first root of J_0 ($k_t a$) = 0, $k_t = 2.405/a$. Consequently, the cutoff frequency for the HE_{11} mode is related to the guide radius a as follows: $f_c = \omega_c/2\pi = 2.405 \cdot c/(2\pi a) = 0.128$ THz.

This cutoff frequency and Eq. (1) offer a good approximation to the dispersion characteristics for the HE_{11} mode in the low-attenuation band (2-3 THz), where the boundary condition $E_x = E_y = 0$ is satisfied. The data deviates from the standard dispersion curve only at frequencies lower than ~1.7 THz, indicating that the spatial profile of the hybrid mode can no longer be described by Eq. (2) and the transverse wavevector $k_t = (2.405/a)$. The simple analytical approximation however holds within the low-attenuation region (2-3 THz).

We conclude that the dispersion relation for the HE_{11} mode is determined primarily by the waveguide bore radius a. The effect of the dielectric layer on dispersion is minimal. Nevertheless the dielectric layer is essential to form the low-loss hybrid modes. The layer thickness determines the frequency band where the transmission loss is reduced and the propagation constant can be approximated by Eq. (1).

It is important to note that the group-velocity dispersion for the HE_{11} and TE_{01} modes is relatively small because the waves travel mostly outside the dielectric in contrast to the surface wave modes on dielectric-coated metal wires and plates. We estimate that the waveguide dispersion parameter D = 0.08 ps/(μm·m) for the HE_{11} mode at 2.3 THz. It corresponds to the pulse broadening of ~1 ps for a 0.15 m long test guide and the pulse bandwidth $\Delta\lambda$ of 80 μm. This figure agrees with the experimentally detected broadening in Fig. 3 (inset). More precise measurements can be performed with longer test waveguides, where the effect of the dielectric becomes noticeable.

4. Summary and conclusions

In summary, the effect of the dielectric layer on structure and dispersion characteristics of the dominant modes in the dielectric-coated cylindrical metallic waveguides was investigated by THz near-field imaging and time-domain spectroscopy.

We show that the dielectric coating forms a set of the linearly-polarized hybrid HE_{1m} modes that match the analytical approximation of Ref. 5. The dielectric layer however has a minimal effect on dispersion of the dominant modes. The phase-velocity of the HE_{11} mode follows the standard dispersion relation in the region of low attenuation (2.0-3.0 THz for the considered waveguides). The cutoff frequency for the HE_{11} mode is determined by the waveguide bore radius and it reflects the boundary condition for the vanishing electric field at the waveguide wall. Note that this cutoff frequency is equal to the cutoff frequency of the TM_{01} mode in a metallic waveguide; however these modes should not be confused because their structures are substantially different. It is also important to note that the dispersion characteristics in the dielectric-coated waveguide do not approach the theoretical curve for the TE_{11} mode at low frequencies despite the fact that the dielectric layer thickness becomes much smaller than the wavelength in the region close to the cutoff frequency. The dielectric-coated waveguides also support the TE_{01} mode with the spatial profile and dispersion characteristics similar to the TE_{01} mode in metallic waveguides.

These findings simplify signal propagation analysis in the dielectric-lined hollow metallic waveguides. We expect that the provided approximation can be used to estimate dispersion in any oversized waveguide ($a >> \lambda$), while more precise evaluation for the dielectric layer effect can be treated by the perturbation theory.

Acknowledgement

We would like to acknowledge A. Fernandez for engaging discussions. This work was supported by the Royal Society [grant number UF080745]; and the Engineering and Physical Sciences Research Council [grant number EP/G033870/1].

#119824 - $15.00 USD Received 10 Nov 2009; revised 4 Dec 2009; accepted 5 Dec 2009; published 15 Jan 2010